First-principles study of misfit strain-stabilized ferroelectric $SnTiO_3$

William D. Parker,[1,*] James M. Rondinelli,[2,†] and S. M. Nakhmanson[1]

[1]*Materials Science Division, Argonne National Laboratory, Argonne, Illinois 60439, USA*

[2]*Department of Materials Science and Engineering, Drexel University, Philadelphia, Pennsylvania 19104, USA*

(Received 9 September 2011; revised manuscript received 30 November 2011; published 27 December 2011)

Toxicity of lead and bismuth has motivated an active search for isovalent ferroelectric oxides free of these elements. Using first-principles density-functional calculations, we survey Sn(II) titanates with $SnTiO_3$ stoichiometry to evaluate the phase stability of polar and nonpolar polymorphs: we predict a tetragonal perovskite $P4mm$ phase with a large axial ratio ($c/a = 1.134$) and ferroelectric polarization (1.28 C/m^2) to be the ground-state equilibrium structure. We also show that heteroepitaxial thin films of perovskite $SnTiO_3$ promote the stereochemical lone-pair activity and simultaneously enable control over the direction of the net electric polarization and magnitude of the electronic band gap. Finally, we examine the consequence of antisite defects on the polar cation displacements by studying the substitution of Sn on Ti sites. We demonstrate that local metallic screening resulting from site substitution diminishes the magnitude of the polar distortions but does not completely quench it. Based on these calculations, we suggest that polar perovskite $SnTiO_3$ ferroelectrics are viable thin-film alternatives to Pb- and Bi-containing oxides.

DOI: 10.1103/PhysRevB.84.245126 PACS number(s): 77.84.−s, 77.80.bn, 77.55.fp, 73.90.+f

I. INTRODUCTION

Many complex materials incorporating $PbTiO_3$ (PTO) as a component, such as $PbZr_{1-x}Ti_xO_3$ (PZT)[1,2] and lead-based relaxor ferroelectrics,[3,4] exhibit colossal piezoelectric responses.[5] These large susceptibilities are routinely exploited in ultrasensitive actuator, sensor, and transducer technologies. The utility of PTO originates mainly from the chemistry of the Pb^{2+} cation: large polar displacements are induced by the nonbonded $6s^2$ electrons, which in turn induce large elastic deformations and electric polarizations. However, multiple environmental issues stemming from the toxicity of lead have incited a search for novel Pb-free ferroelectrics with cation displacements of comparable (or greater) magnitude for next-generation sustainable electroactive materials.[6–8]

Recently, several computational studies[9–11] have suggested isovalent substitution of environmentally benign Sn(II) for lead in titanate perovskites since the behavior of Sn^{2+} is also governed by strong electron lone-pair activity.[12,13] Indeed, these investigations[9–11] predict that the $5s^2$ lone pair is stereochemically active in perovskite-structured $SnTiO_3$ and responsible for the polar tetragonal (space group $P4mm$) structure exhibiting piezoelectric[10] and ferroelectric[10,11] properties that are similar to or exceed those of bulk PTO. Nevertheless, the practical potential for tetragonal perovskite $SnTiO_3$ to replace PTO remains unclear as there are a number of other polymorphs with ABO_3 stoichiometry that may be energetically more favorable. In fact, two studies[14,15] suggest that bulk perovskite $SnTiO_3$ is metastable with respect to a hexagonal (nonpolar, $R\bar{3}$) ilmenite polymorph but strongly disagree on the extent of the energy stabilization. Stability of the ilmenite $SnTiO_3$ polymorph is surprising since centrosymmetric structures containing Sn^{2+} would be highly susceptible to cooperative pseudo-Jahn-Teller (PJT) distortions that disfavor inversion symmetry.[16] Thus polar phases of Sn(II) titanates should be energetically preferable over the nonpolar ones.

Conventional solid-state growth of bulk Sn(II)-based oxides remains extremely challenging as most synthetic routes for producing ceramic $SnTiO_3$ require high temperatures. Consequently, facile Sn^{2+} disproportionation into Sn^{4+} and Sn metal often occurs,[11,17] leading to the loss of electron lone pair activity (along with the polar distortions) and thus *centrosymmetric* crystal structures. Modern state-of-the-art epitaxial engineering techniques offer an alternative avenue to avoid the restrictions imposed by bulk thermodynamics during growth: they can stabilize metastable structures through artificial elastic boundary conditions (misfit strain) and/or rate-limited kinetics.[18] However, a recent attempt to grow tin titanate films on sapphire and perovskite substrates from ceramic SnO_2 and TiO_2 targets utilizing pulsed laser deposition (PLD) techniques yielded nonpolar ilmenite-type structures with only traces of a second phase compatible with perovskite geometry.[19] This result suggests that either the $SnTiO_3$ stoichiometry or the Sn^{2+} oxidation state (or both) were not sufficiently achieved in the PLD-grown films. Thus the uncertainty about the nature of the ground state of $SnTiO_3$ and the lack of information on whether or not the proposed polar-perovskite phase could be stabilized by epitaxial techniques readily motivates a thorough investigation of potential polymorph phases.

In this study, we use first-principles density-functional theory (DFT) calculations to examine the structural stability of tin titanate polymorphs with $SnTiO_3$ stoichiometry. We find that the low-energy phases are perovskite, possessing corner-sharing TiO_6 octahedra and polar cation displacements. We then evaluate the relative phase stability of these polar perovskite structures under biaxial strain, showing that the elastic strain energy induced by lattice mismatch with the substrate promotes the stereochemical lone-pair activity and simultaneously enables control over the direction of the net electric polarization. Finally, we demonstrate that antisite point defect pairs, namely the substitution of Sn on a Ti site (Sn_{Ti} + Ti_{Sn}), motivated by the propensity for tin to exist in the 4+ oxidation state, lead to metallic behavior from the partial occupation of the formerly empty Ti d bands. This metallic screening decreases the repulsion between the Sn^{2+} lone pairs and oxygen atoms and subsequently reduces the magnitude of the cooperative polar distortions.

II. COMPUTATIONAL DETAILS

DFT calculations were performed using the QUANTUM ESPRESSO package[20] within the local-density approximation (LDA), parametrized by Perdew and Zunger,[21] and the generalized gradient approximation (GGA) of Perdew and Wang (PW91).[22] The electronic wave functions (density) were expanded in plane waves up to 30 Ry (300 Ry), and the core and valence electrons were treated with Vanderbilt ultrasoft[23] pseudopotentials.[24] Shifted Monkhorst-Pack (MP)[25] meshes were used for the Brillouin-zone (BZ) integrations and for phonon-band calculations with an $8 \times 8 \times 8$ mesh utilized for a five-atom perovskite unit cell and rescaled accordingly for larger unit cells.

For evaluating the structural stability of the perovskite polymorphs, we employed density-functional perturbation theory[26] to compute phonon-band dispersions. Starting from the high-symmetry nonpolar configuration, we systematically froze in linear combinations of the obtained unstable phonon-mode eigenvectors and then performed structural relaxations from these initial atomic configurations to reach the ground-state configuration. All internal ionic positions were relaxed until the forces were less than 0.4×10^{-3} Ry bohr^{-1} ($\sim$0.01 eV/Å). We simulated epitaxial thin-film constraints on a cubic (001)-oriented substrate by varying the in-plane lattice constant a of a tetragonal perovskite cell and allowing the out-of-plane lattice constant c to relax (to stresses less than 0.5 kbar). The biaxial misfit strain is defined as $\varepsilon = a/a_0 - 1$, where a_0 corresponds to the LDA-optimized cubic $Pm\bar{3}m$ lattice parameter. For all polar structures, the Berry-phase (BP) method[27] was used to calculate the total electric polarization.

III. POLYMORPH ANALYSIS

We first explore the stability of various $SnTiO_3$ polymorphs by calculating their optimized structures within the LDA. Plausible polymorphs include polar and nonpolar perovskites and trigonal $R3c$ [lithium niobate (LN in what follows)] phases, all of which have corner-sharing TiO_6 octahedra. Layered hexagonal phases are also feasible: we consider $R\bar{3}$ (ilmenite), $P6_3/mmc$, and $P6_3mc$ structures, the former containing edge-sharing and the latter two face-sharing TiO_6 octahedral networks.

The connectivity of the octahedral network strongly affects the presence or absence of polar distortions in a given polymorph.[28,29] We find that the phases with corner-sharing octahedra are, in general, more stable than the hexagonal polymorphs (Table I). The polar perovskite ($P4mm$) phase has the lowest energy of all structures, and the two other low-energy phases are monoclinic perovskite Cm and LN-type $R3c$.

Since ferroelectric distortions in perovskites are known to be sensitive to unit-cell volumes,[30,31] we recompute the energetic hierarchy among these phases using the GGA exchange-correlation functional and re-relax the atomic structures to be fully self-consistent. As observed elsewhere,[32,33] GGA calculations of ferroelectric oxides favor larger lattice constants as well as some enhanced c/a ratios (Table I). We also find that the energy of the LN-type $R3c$, $R\bar{3}$, Cm, and $Pm\bar{3}m$ phases increases and that of the $P6_3mc$ and $P6_3/mmc$ phases decreases compared to the LDA results. Nevertheless, the energetic ordering of phases from low to high remains the same regardless of the exchange-correlation functional, suggesting that the susceptibility to polar distortions in corner-sharing $SnTiO_3$ polymorphs is robust.

TABLE I. Energy differences (ΔE) per formula unit (f.u.) for various $SnTiO_3$ polymorphs with respect to the polar perovskite $P4mm$ phase, which has the lowest energy. Results for the LDA (and GGA) exchange-correlation functionals are given (in parentheses). The first four structures possess corner-sharing TiO_6 octahedra while the last three contain edge- or face-sharing octahedra. The total electric polarization **P** is also provided for the polar crystal structures.

Symmetry	ΔE (eV/f.u.)	a (Å)	c/a	**P** (C/m^2)
$P4mm$	0.00 (0.00)	3.78 (3.85)	1.13 (1.15)	1.28
Cm	0.03 (0.10)	3.90 (3.99)	1.00 (1.00)	1.08
$R3c$ (LN)	0.03 (0.06)	5.50 (5.61)	2.48 (2.51)	1.08
$Pm\bar{3}m$	0.32 (0.43)	3.86 (3.94)	1.00 (1.00)	
$R\bar{3}$	0.43 (0.47)	5.37 (5.44)	2.75 (2.83)	
$P6_3/mmc$	0.91 (0.90)	5.48 (5.59)	1.69 (1.69)	
$P6_3mc$	2.00 (1.78)	5.37 (5.50)	1.00 (0.93)	

The energetic near-degeneracy of the Cm and LN-type $R3c$ phases calls for a closer inspection of these structures (Table I). Figure 1 shows the pair distribution functions (PDFs) $g(r)$ of the $P4mm$, Cm, and LN-type $R3c$ polymorphs. The plots for the two latter structures look nearly identical up to a distance of 3 Å. At the same time, both of them are markedly different from the PDF plot of the $P4mm$ structure. This indicates that the local Ti-O and Sn-O environments, including the polar cation off-centering motifs, of the Cm and LN-type $R3c$ structures are practically the same. In the LN-type polymorph, the formerly octahedral Sn-O cages become highly distorted, making Sn nine-coordinated, similar to the perovskite structures. Such

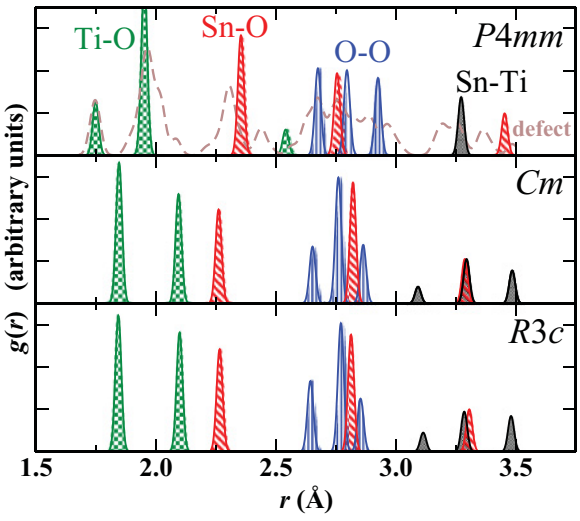

FIG. 1. (Color online) Pair distribution functions (PDFs) $g(r)$ of the three lowest-energy $SnTiO_3$ polymorphs, $P4mm$, Cm, and LN-type $R3c$, resolved by pair atomic types (black/shaded for Sn-Ti, red/diagonal-striped for Sn-O, green/checkered for Ti-O, and blue/vertical-striped for O-O). The PDF of the Sn-Ti substitutional defect (see Sec. VII) is indicated by the dashed line in the $P4mm$ frame.

structural similarity among these different space groups, however, should not be considered unusual given that the perovskite and LN-type phases are closely related, as pointed out early on by Megaw.[34] Nonetheless, since the Cm and LN-type $R3c$ phases (both highly polar as shown in Sec. V) are energetically close to the ground-state $P4mm$ phase, it should be possible to stabilize either one of them in epitaxial synthesis by an appropriate choice of a substrate (e.g., sapphire in the case of the hexagonal LN-type structure).

IV. EPITAXIAL STRAIN STABILIZATION

Here we explore the simplest case of perovskite $SnTiO_3$ films on cubic (001)-perovskite substrates[35] to evaluate the effect of epitaxial strain on the perovskite phase stability and ferroelectric polarization. In Fig. 2, we present the calculated phonon frequencies for the paraelectric five-atom perovskite structure under different biaxial strain states within the LDA. We find multiple structural instabilities, including ferroelectric (FE), antiferroelectric (AFE), and antiferrodistortive (AFD) modes in the epitaxially strained tetragonal structures.

The FE instabilities are the strongest and depend linearly on the applied strain. The out-of-plane–oriented A_{2u} mode dominates for epitaxial compression ($\varepsilon \leqslant 0$), and the doubly degenerate in-plane E_u mode dominates for epitaxial tension ($\varepsilon \geqslant 0$). The Γ-point phonon frequencies and the Born effective charge (BEC) tensor components that we obtain for the epitaxially relaxed $P4mm$ structure agree with the results reported by Uratani *et al.*[10]

The AFD modes also change linearly with epitaxial strain. The strongest TiO_6 rotation instabilities always lie $\sim$50 cm^{-1} higher than the strongest FE mode. This suggests that the ground-state epitaxial phases are likely free of AFD distortions—we confirm this by performing phonon-band calculations of the polar structures. Finally, we note that the AFE modes exhibit a highly nonlinear strain dependence, becoming unstable only for strains in excess of $\pm 1\%$. Although, for the considered strain interval, the AFE modes are always weaker than the FE and AFD instabilities, they may become more important at larger strains.

A. Compressive strain

Freezing in the FE_z (A_{2u}) mode in epitaxially compressed structures lowers the symmetry from $P4/mmm$ to $P4mm$, compatible with a nonzero polarization $\mathbf{P} = (0,0,P_z)$. Recomputing the phonon-band dispersions in the $P4mm$ epitaxial structures reveals no remaining structural instabilities. The condensation of the FE mode hardens the AFD and AFE instabilities present in the paraelectric structure. Increasing compressive strain leads to an enhanced polarization (Fig. 3) driven mostly by tin moving along the z direction away from its high-symmetry position: the average Sn displacement is $\sim$0.5 Å while the Ti cation displacements are always smaller (<0.1 Å).

B. Tensile strain

Freezing in the FE_{xy} (E_u) modes in the paraelectric perovskite $SnTiO_3$ structure under tensile strain produces a lower symmetry phase (space group $Amm2$) with polar distortions

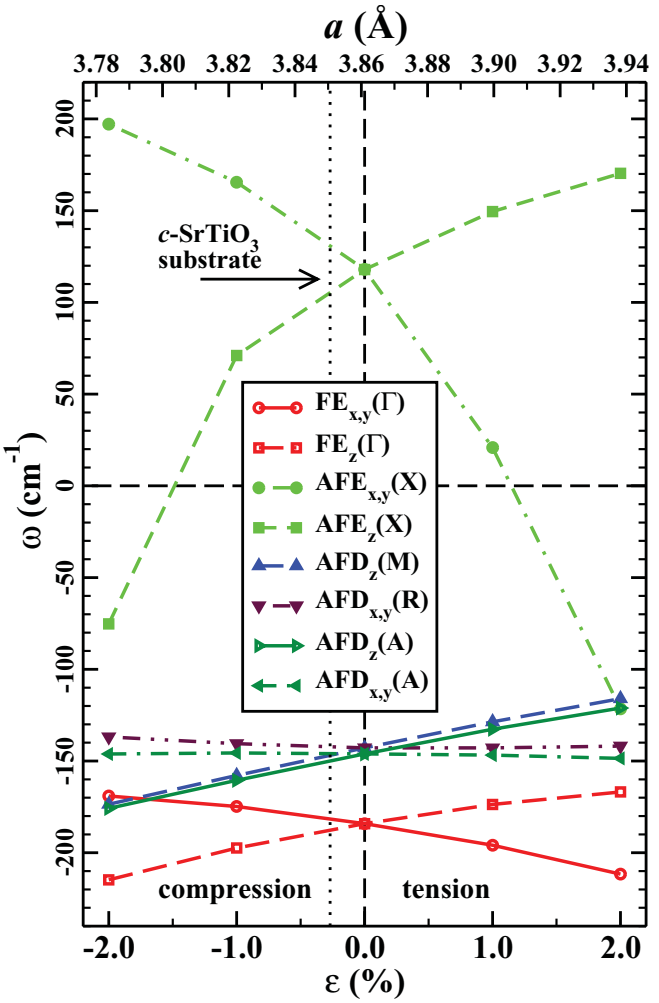

FIG. 2. (Color online) Unstable phonon-mode frequencies ω at Γ and various (tetragonal) BZ-boundary $\mathbf{q}$ points of the paraelectric perovskite $SnTiO_3$ under biaxial strain ε. Imaginary frequencies associated with unstable modes are plotted as negative numbers below the horizontal zero line. $\mathbf{q}$ points $X = (\frac{1}{2},0,0)$, $M = (\frac{1}{2},\frac{1}{2},0)$, $R = (\frac{1}{2},0,\frac{1}{2})$, or $A = (\frac{1}{2},\frac{1}{2},\frac{1}{2})$ are marked in brackets after the instability label subscripts, which indicate the sense of direction: axial (α) or (α,β) ionic motion for the FE and AFE ones, single (α) or an equivalent set (α,β) of rotational axes for the AFD ones; here $\alpha,\beta = x,y,z$.

present in equal amplitudes in plane, i.e., $\mathbf{P} = (P_x, P_y \equiv P_x, 0)$. However, for all tensile strain states, an unstable polar zone-center phonon (FE_z) mode persists. Subsequently freezing in this distortion leads to a further energy reduction (60 meV/f.u.) and lifts the ferroelectric polarization out of the plane, lowering the crystal symmetry to the Cm space group compatible with $\mathbf{P} = (P_x, P_y \equiv P_x, P_z \neq P_x)$. Thus, despite epitaxy on a two-dimensional (2D) square net, polarization in these structures orients itself along a non-Cartesian direction. This behavior contrasts with that of epitaxially strained $SrTiO_3$, where only an in-plane polarization develops under tensile strain.[36] Our observation of an out-of-plane polarization component in strained $SnTiO_3$ is likely the result of an active lone pair on Sn^{2+}. Note that additional instability analysis of the Cm structures reveals no unstable phonon modes in the BZ,

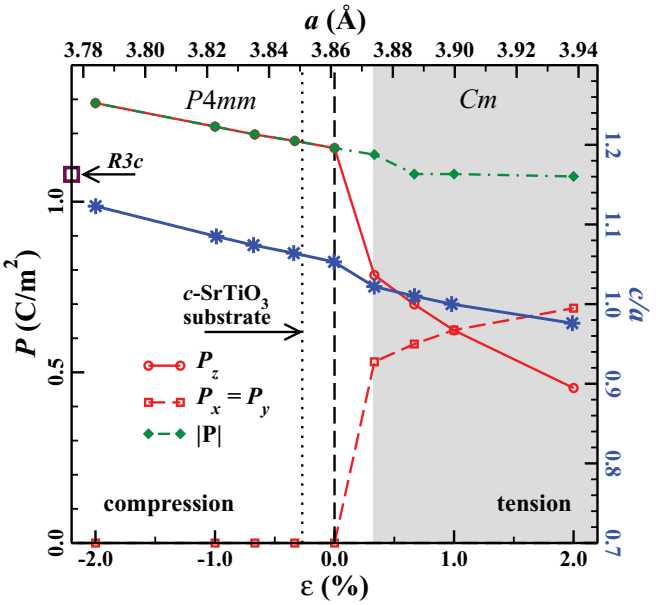

FIG. 3. (Color online) Polarization (left vertical axis) and tetragonality (right vertical axis, star data points) of epitaxially strained $P4mm$ and Cm $SnTiO_3$ phases as functions of biaxial misfit strain ε. Polarization of the $R3c$ LN-type structure is also marked on the left as an open square for comparison. The shaded area outlines the region of the Cm phase stability.

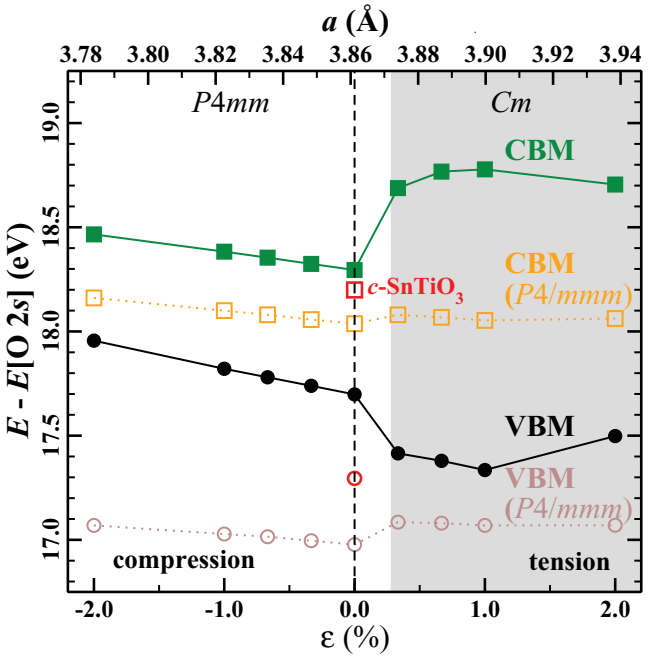

FIG. 4. (Color online) Valence-band maxima (VBM) [circles] and conduction-band minima (CBM) [squares] of epitaxially strained $P4mm$ and Cm $SnTiO_3$ phases as functions of biaxial strain. Data for the corresponding $P4/mmm$ structures are also shown in dotted lines. Open (red) square and circle at zero strain mark the VBM and CBM positions in the cubic $Pm\bar{3}m$ structure.

indicating that they are also dynamically stable. Compared to the compressively strained $P4mm$ structures, the tensile-strained Cm structures have Sn displacements of ~0.4 Å along noncrystallographic directions and Ti displacements opposite to Sn ~0.1 Å.

V. POLARIZATION AND TETRAGONALITY

The evolution in the c/a ratio and polarization vector components with epitaxial strain in perovskite $SnTiO_3$ is summarized in Fig. 3. (The polarization of the $R3c$ LN-type structure is also shown for comparison.) According to our calculations, the strained polar structures of $SnTiO_3$ have polarization in excess of 0.9 C/m^2 throughout the whole range of applied strains. The total polarization values for the Cm and LN-type $R3c$ phases are comparable as expected from their structural similarity. In the $P4mm$ phases, high polarization is accompanied by large tetragonality, which reaches 1.134 in the stress-free[37] structure (Table I). Even at 2% tensile strain, the P_z component in the Cm phase remains rather large (~40% of the total polarization), suggesting that, unlike isovalent $SrTiO_3$, even small tensile strains possess switchable and addressable out-of-plane polarizations. The polarization values obtained for all the polar $SnTiO_3$ phases and especially the tetragonality of the $P4mm$ structures are higher than those computed for PTO with the same methodology.[1]

VI. STRAIN DEPENDENCE OF ELECTRONIC PROPERTIES

The electronic properties of the stress-free polar-perovskite $P4mm$ phase of $SnTiO_3$ have been thoroughly investigated elsewhere.[9–11] Our calculations of the electronic band structure as well as the total and projected density of states (PDOS) of the same phase are in good agreement with the aforementioned works. In this section, we focus on the electronic structure of the *biaxially* strained perovskite phases.

Figure 4 shows the changes in position of the valence-band maximum (VBM) formed by O $2p$ states and the conduction-band minimum (CBM) with Ti d-character (computed within DFT/LDA) as the system transforms from $P4mm$ to Cm symmetry under applied strain. Similar dependencies for the high-symmetry $P4/mmm$ structure are also shown to isolate the influence of the elastic distortion of the nonpolar (clamped-ion) tetragonal cell on the VBM and CBM positions. In all cases, the shifts of the energy levels are referenced with respect to the low-lying O $2s$ state, which is assumed to be undisturbed by any distortions. The band gaps $E_{gap} \equiv E_{VBM} - E_{CBM}$ obtained for all the structures above are indirect, the VBM and CBM located at X and Γ points, respectively.[38]

The nonpolar clamped-ion cell distortion alone has a negligible influence on the size of E_{gap}. When the $P4mm$ polar ionic distortion is introduced, the VBM and CBM only undergo a rigid shift, compared to their positions in the $P4/mmm$ structure. In contrast, the VBM and CBM in Cm exhibit a more complicated behavior—in addition to the rigid shift, the E_{gap} opens up by >0.5 eV.

The large change in the band gap E_{gap} originates from the sensitivity of the conduction band to applied strain, in particular, the Ti d_{xy} orbital level (Fig. 5). The change in the cubic crystal-field symmetry induced by the polar ionic displacements shifts this level down for compressive strains such that the d_{xy} orbital forms the bottom of the conduction

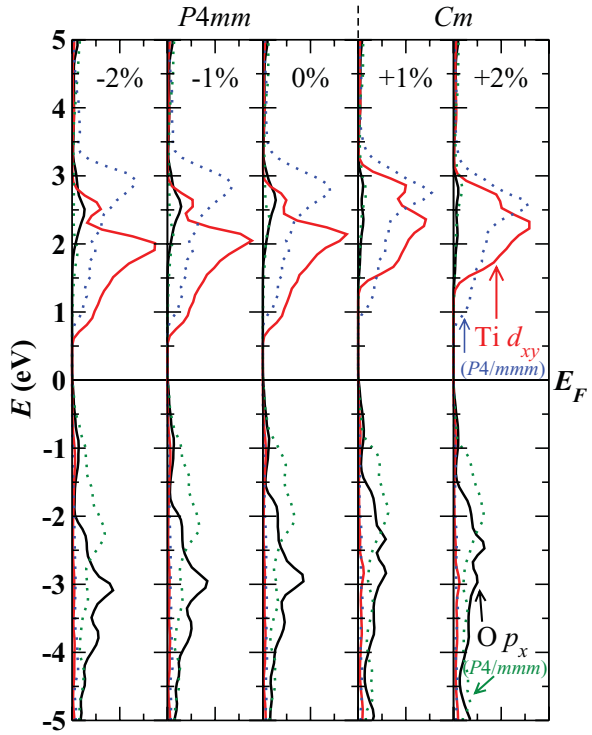

FIG. 5. (Color online) Evolution of the Ti d_{xy} and O p_x orbital projected density of states (PDOS) in epitaxially strained $P4mm$ and Cm $SnTiO_3$ with biaxial strain. Data for the corresponding $P4/mmm$ structures are also shown in dotted lines. See Sec. VI for more details.

band at the Γ point. On the other hand, tensile strains push the d_{xy} orbital to higher energies so that the CBM is formed by the $d_{xz,yz}$ states.[39] The strength of the interaction between the Ti d_{xy} and the O $p_{x,y}$ orbitals determines the size of the gap. Under compressive strain, the $P4mm$ structure retains a fourfold rotational symmetry element, which prevents the hybridization of the Ti d_{xy} state and the O $p_{x,y}$ states (at the Γ point), suppressing further broadening of the E_{gap}. In contrast, under tensile strain, the fourfold symmetry is lifted by the polar displacements. This distortion allows the Ti d_{xy} and the O $p_{x,y}$ states to mix at the Γ point. The mixing leads to an additional repulsion between the VBM and CBM, which opens up the band gap.

The strong dependence of the size of E_{gap} on the direction of **P** opens up interesting opportunities for dynamical tuning of it by growing $SnTiO_3$ films under an epitaxial condition that is close to the boundary between the $P4mm$ and Cm phases, e.g., on a $SrTiO_3$ substrate. E_{gap} tuning is accessible elastically, by flexing the substrate, or electrically, by applying an electric field. Because the gap opening mechanism presented here is quite generic, it should also work in epitaxially strained PTO. We speculate, however, that, in $SnTiO_3$, the effect should be more pronounced since the polar displacements in the present case are larger than in $PbTiO_3$.

VII. ANTISITE DEFECTS

Since tin is readily found in a 4+ electronic configuration with a sixfold ionic radius (0.69 Å) close to that of Ti^{4+} (0.61 Å), it is conceivable that, in the perovskite structure, Sn(IV) could be found on the Ti site. To evaluate the effect of such antisite defects on the atomic distortions responsible for the ferroelectric polarization, we construct a $2 \times 2 \times 2$ (40-atom) supercell starting from bulk polar $P4mm$ phase and put one Sn (and Ti) atom on a Ti (and Sn) site, corresponding to a 12.5% defect concentration. We then fully relax the lattice constants and atomic positions until force and stress convergence is achieved at fixed composition, i.e., $(Sn_7, Ti)(Ti_7, Sn)O_{24}$.

We find that the crystal symmetry of the tin titanate with an antisite cation defect reduces to Cm, similar to the structure under tensile epitaxial strain and compatible with a polarization not aligned along a crystallographic direction. Locally, we observe a contraction of all of the Sn-O bonds at the Sn sites adjacent to the Sn_{Ti} defect, producing a sevenfold cation coordination. In defect-free $P4mm$ and on the Sn sites of the defect structure, Sn displaces away from the center of the O-coordination sphere, but, when Sn sits on the Ti site in the substitutional defect structure, the Sn atom remains in the center. This lack of Sn displacement in a 4+ oxidation state indicates that a lone pair of electrons drives the polar distortion. The shift in the PDF of the defect structure to smaller distances indicates a reduction in lone-pair activity (top panel of Fig. 1). Indeed, our LDA band-structure calculations reveal that the antisite defects produce a metallic ground state from partial electron doping into the conduction band. This metallic screening reduces the Coulomb repulsion between the coordinating oxygen atoms and the electron lone pair, which is still present and shifts into the xy plane, allowing the Sn atoms to move closer to the oxygen atoms. Interestingly, the antisite defects also lead to an increase in the Sn-O bond lengths in the square antiprismatic coordinations, which remain in the planes above and below the Sn_{Ti} defect site. Moreover, the octahedrally coordinated Sn at the Ti site also exhibits a polar displacement comparable in magnitude to those of the Ti atoms despite the presumed absence of lone-pair activity—these displacements produce the shoulder in the PDF peak near 2.0 Å (Fig. 1). The polar structure therefore persists in the presence of the antisite defects. These antisite defects are thus not detrimental to the ferroelectric distortions but do introduce channels for electron conduction that could make polarization measurements challenging. We suggest that the ferroelectricity should be robust for smaller concentrations of cation defects of the type explored here. A more exhaustive search for competing defect-pair combinations would be useful.

VIII. CONCLUSIONS

Although we do not specify the growth conditions necessary to stabilize perovskite $SnTiO_3$, our investigation reveals that it should be possible to achieve a ferroelectric (i.e., both highly polar and switchable) structure through modern atomic layer deposition (ALD) techniques. In particular, an appropriate technique should be capable of maintaining a strict ABO_3 stoichiometry—a challenge under reducing conditions due to the high vapor pressure of tin—and enforcing the 2+ oxidation state of tin during growth to preserve the electron lone-pair activity driving the polar structural distortions. An additional benefit of employing ALD epitaxial synthesis is that the very large tetragonality of the bulk $P4mm$ structure, which may prohibit polarization switching by a reasonable coercive

field,[40] could be reduced by judicious selection of a less compressive substrate without sacrificing strong polarization in the out-of-plane direction (see Fig. 3).

As shown here and in Refs. 9–11, between the Sn^{2+} lone pairs in $SnTiO_3$ resembles that of Pb^{2+} in PTO and is governed by the strong electron lone-pair activity.[12,13] We have demonstrated that polar polymorphs of $SnTiO_3$, including perovskites and the LN-type structure, are energetically preferable over the nonpolar ones, as expected for the strongly distortive Sn^{2+} ion from theoretical considerations of the cooperative-PJT effect.[16] We have also shown that epitaxially stabilized perovskite phases of $SnTiO_3$ are highly polar and possess large out-of-plane polarization at *both* compressive and tensile strains, making them more functional than $SrTiO_3$ films, especially under tensile strain. The transformation between the epitaxially stabilized polar perovskite phases also induces large changes in the band gap of $SnTiO_3$. Finally, the similarity of the electronic properties of Sn^{2+} and Pb^{2+} should make it possible to fabricate lead-free layered-oxide epitaxial films exhibiting Goldstone-like excitations.[41]

ACKNOWLEDGMENTS

This project was supported by the US Department of Energy, Office of Science, Office of Basic Energy Sciences, and by American Recovery and Reinvestment Act (ARRA) funding through the Office of Advanced Scientific Computing Research under Contract No. DE-AC02-06CH11357.

*wparker@anl.gov
†Also at X-Ray Science Division, Argonne National Laboratory, Argonne, Illinois 60439, USA.

[1] H. N. Lee, S. M. Nakhmanson, M. F. Chisholm, H. M. Christen, K. M. Rabe, and D. Vanderbilt, Phys. Rev. Lett. **98**, 217602 (2007).
[2] M. Ahart, R. E. Cohen, P. Ganesh, P. Dera, H.-K. Mao, R. J. Hernley, Y. Ren, P. Liermann, and Z. Wu, Nature (London) **451**, 545 (2008).
[3] S.-E. Park and T. R. Shrout, J. Appl. Phys. **82**, 1804 (1997).
[4] Z. Kutnjak, J. Petzelt, and R. Blinc, Nature (London) **441**, 956 (2006).
[5] B. Noheda, Curr. Opin. Solid State Mater. Sci. **6**, 27 (2002).
[6] Y. Saito, H. Takao, T. Tani, T. Nonoyama, K. Takatori, T. Homma, T. Nagaya, and M. Nakamura, Nature (London) **432**, 84 (2004).
[7] J. W. Bennett, I. Grinberg, P. K. Davies, and A. M. Rappe, Phys. Rev. B **83**, 144112 (2011).
[8] R. Armiento, B. Kozinsky, M. Fornari, and G. Ceder, Phys. Rev. B **84**, 014103 (2011).
[9] Y. Konishi, M. Ohsawa, Y. Yonezawa, Y. Tanimura, T. Chikyow, H. Koinuma, A. Miyamoto, M. Kubo, and K. Sasata, *Possible Ferroelectricity in SnTiO$_3$ by First-Principles Calculations*, MRS Proceedings 748 (Materials Research Society, Pittsburgh, 2003), p. U3.13.1.
[10] Y. Uratani, T. Shishidou, and T. Oguchi, Jpn. J. Appl. Phys. **47**, 7735 (2008).
[11] S. Matar, I. Baraille, and M. Subramanian, Chem. Phys. **355**, 43 (2009).
[12] G. W. Watson and S. C. Parker, J. Phys. Chem. B **103**, 1258 (1999); G. W. Watson, S. C. Parker, and G. Kresse, Phys. Rev. B **59**, 8481 (1999); G. W. Watson, J. Chem. Phys. **114**, 758 (2001).
[13] A. Walsh and G. W. Watson, Phys. Rev. B **70**, 235114 (2004).
[14] A. Lebedev, Phys. Solid State **51**, 362 (2009).
[15] G. Hautier, C. C. Fischer, A. Jain, T. Mueller, and G. Ceder, Chem. Mater. **22**, 3762 (2010).
[16] I. B. Bersuker, Ferroelectrics **164**, 75 (1995); *The Jahn-Teller Effect* (Cambridge University Press, Cambridge, England, 2006).
[17] M. S. Moreno, G. Punte, G. Rigotti, R. C. Mercader, A. D. Weisz, and M. A. Blesa, Solid State Ionics **144**, 81 (2001).
[18] P. A. Salvador, T.-D. Doan, B. Mercey, and B. Raveau, Chem. Mater. **10**, 2592 (1998).
[19] T. Fix, S.-L. Sahonta, V. Garcia, J. L. MacManus-Driscoll, and M. G. Blamire, Cryst. Growth Des. **11**, 1422 (2011).
[20] P. Giannozzi, S. Baroni, N. Bonini, M. Calandra, R. Car, C. Cavazzoni, D. Ceresoli, G. L. Chiarotti, M. Cococcioni, I. Dabo, A. D. Corso, S. de Gironcoli, S. Fabris, G. Fratesi, R. Gebauer, U. Gerstmann, C. Gougoussis, A. Kokalj, M. Lazzeri, L. Martin-Samos, N. Marzari, F. Mauri, R. Mazzarello, S. Paolini, A. Pasquarello, L. Paulatto, C. Sbraccia, S. Scandolo, G. Sclauzero, A. P. Seitsonen, A. Smogunov, P. Umari, and R. M. Wentzcovitch, J. Phys.: Condens. Matter **21**, 395502 (2009).
[21] J. P. Perdew and A. Zunger, Phys. Rev. B **23**, 5048 (1981).
[22] J. P. Perdew, J. A. Chevary, S. H. Vosko, K. A. Jackson, M. R. Pederson, D. J. Singh, and C. Fiolhais, Phys. Rev. B **46**, 6671 (1992), this work uses the designation GGA-PW II for PW91; **48**, 4978 (1993).
[23] D. Vanderbilt, Phys. Rev. B **41**, 7892 (1990).
[24] For the LDA, the pseudopotentials have the following parameters: Sn: $4d^{10}5s^25p^2$, $r_0 = 1.1$ bohr, $r_c^{\rm loc} = 2.4$ bohr, $r_c = (2.2, 2.5, 2.5)$ bohr for d, s, and p, respectively; Ti: $3s^23p^64s^23d^1$, $r_0 = 1.0$ bohr, $r_c^{\rm loc} = 1.8$ bohr, $r_c = (1.8, 1.8, 1.8)$ bohr for s, p, and d, respectively; O: $2s^22p^4$, $r_0 = 0.7$ bohr, $r_c^{\rm loc} = 1.0$ bohr, $r_c = (1.3, 1.3)$ bohr for s and p, respectively. For PW91, the pseudopotentials have the same valence configurations and $r_c^{\rm loc}$ as for the LDA, with the exception of the Sn $r_c = (1.7, 2.0, 2.2)$ a.u., and the O $r_c = (1.2, 1.2)$ a.u.
[25] H. J. Monkhorst and J. D. Pack, Phys. Rev. B **13**, 5188 (1976).
[26] S. Baroni, S. de Gironcoli, A. Dal Corso, and P. Giannozzi, Rev. Mod. Phys. **73**, 515 (2001).
[27] R. D. King-Smith and D. Vanderbilt, Phys. Rev. B **49**, 5828 (1994).
[28] M. Kunz and I. D. Brown, J. Solid State Chem. **115**, 395 (1995).
[29] P. S. Halasyamani, Chem. Mater. **16**, 3586 (2004).
[30] K. M. Rabe, *Computer Simulation Studies in Condensed-Matter Physics XVI*, edited by D. P. Landau, S. P. Lewis, and H.-B. Schüttler, Springer Proceedings in Physics No. 95 (Springer, New York, 2003), pp. 213–225.
[31] T. Nishimatsu, M. Iwamoto, Y. Kawazoe, and U. V. Waghmare, Phys. Rev. B **82**, 134106 (2010).
[32] D. I. Bilc, R. Orlando, R. Shaltaf, G.-M. Rignanese, J. Íñiguez, and P. Ghosez, Phys. Rev. B **77**, 165107 (2008).
[33] R. Wahl, D. Vogtenhuber, and G. Kresse, Phys. Rev. B **78**, 104116 (2008).
[34] H. D. Megaw, *Crystal Structures: A Working Approach*, Studies in Physics and Chemistry (Saunders, Philadelphia, 1973).
[35] J. M. Rondinelli and N. A. Spaldin, Adv. Mater. **23**, 3363 (2011).
[36] J. H. Haeni, P. Irvin, W. Chang, R. Uecker, P. Reiche, Y. L. Li, S. Choudhury, W. Tian, M. E. Hawley, B. Craigo, A. K. Tagantsev, X. Q. Pan, S. K. Streiffer, L. Q. Chen, S. W. Kirchoefer, J. Levy, and D. G. Schlom, Nature (London) **430**, 758 (2004).

[37] $\sigma_{\alpha\alpha} \rightarrow 0$ ($\alpha = x,y,z$) as opposed to the strained structure where only $\sigma_{zz} \rightarrow 0$.

[38] At $+1\%$ strain, the CBM of the Cm structure moves slightly away from Γ in the direction of X, and, at $+2\%$ strain, the VBM of the Cm structure moves to Z, instead of X.

[39] In the nonpolar $P4/mmm$ structure (dotted lines in Fig. 5), biaxial strain induces a tetragonal crystal-field distortion that splits the $3d$ orbital degeneracies differently than in polar structures: The energies of the $d_{xz,yz}$ orbitals are lowered under compressive strains, whereas the d_{xy} orbital energy is lowered at tensile strains.

[40] M. R. Suchomel, A. M. Fogg, M. Allix, H. Niu, J. B. Claridge, and M. J. Rosseinsky, Chem. Mater. **18**, 4987 (2006).

[41] S. M. Nakhmanson and I. Naumov, Phys. Rev. Lett. **104**, 097601 (2010).